# Direct Voltammetric Observation of Redox Driven Changes in Axial Coordination and Intramolecular Rearrangement of the Phenylalanine-82-Histidine Variant of Yeast Iso-1-cytochrome *c*[†]

Benjamin A. Feinberg,*[,§] Xiangjun Liu,[‖] Michael D. Ryan,*[,‡] Abel Schejter,[⊥] Chongyao Zhang,[§] and Emanuel Margoliash[‖]

*Department of Chemistry, University of Wisconsin−Milwaukee, 3210 North Cramer Street, Milwaukee, Wisconsin 53211, Laboratory for Molecular Biology (M/C 066), Department of Biological Sciences, University of Illinois at Chicago, 845 West Taylor Street, Chicago, Illinois 60607-7060, Department of Chemistry, Todd Wehr Chemistry Building, Marquette University, Milwaukee, Wisconsin 53233, and Sackler Institute of Molecular Medicine, Sackler School of Medicine, Tel-Aviv University, Tel-Aviv, Israel 69978*

*Received May 5, 1998; Revised Manuscript Received July 20, 1998*

ABSTRACT: Direct square-wave and cyclic voltammetric electrochemical examination of the yeast iso-1-cytochrome *c* Phe82His/Cys102Ser variant revealed the intricacies of redox driven changes in axial coordination, concomitant with intramolecular rearrangement. Electrochemical methods are ideally suited for such a redox study, since they provide a direct and quantitative visualization of specific dynamic events. For the iso-1-cytochrome *c* Phe82His/Cys102Ser variant, square-wave voltammetry showed that the primary species in the reduced state is the $Met_{80}$-$Fe^{2+}$-$His_{18}$ coordination form, while in the oxidized state the $His_{82}$-$Fe^{3+}$-$His_{18}$ form predominates. The addition or removal of an electron to the appropriate form of this variant serves as a switch to a new molecular form of the cytochrome. Using the $2 \times 2$ electrochemical mechanism, simulations were done for the cyclic voltammetry experiments at different scan rates. These, in turn, provided relative rate constants for the intramolecular rearrangement/ligand exchange and the equilibrium redox potentials of the participating coordination forms: $k_{b,AC} = 17\ s^{-1}$ for $Met_{80}$-$Fe^{3+}$-$His_{18} \rightarrow His_{82}$-$Fe^{3+}$-$His_{18}$ and $k_{f,BD} > 10\ s^{-1}$ for $His_{82}$-$Fe^{2+}$-$His_{18} \rightarrow Met_{80}$-$Fe^{2+}$-$His_{18}$; $E^{0\prime} = 247$ mV for $Met_{80}$-$Fe^{3+/2+}$-$His_{18}$ couple, $E^{0\prime} = 47$ mV for $His_{82}$-$Fe^{3+/2+}$-$His_{18}$ couple, and $E^{0\prime} = 176$ mV for the cross-reaction couple, $His_{82}$-$Fe^{3+}$-$His_{18} + e^- \rightarrow Met_{80}$-$Fe^{2+}$-$His_{18}$. Thermodynamic parameters, including the entropy of reaction, $\Delta S^{0\prime}_{Rxn}$, were determined for the net reduction/rearrangement reaction, $His_{82}$-$Fe^{3+}$-$His_{18} + e^- \rightarrow Met_{80}$-$Fe^{2+}$-$His_{18}$, and compared to those for wild-type cytochrome, $Met_{80}$-$Fe^{3+}$-$His_{18} + e^- \rightarrow Met_{80}$-$Fe^{2+}$-$His_{18}$. For the Phe82His variant mixed redox couple, $\Delta S^{0\prime}_{Rxn} = -80$ J/mol·K compared to $\Delta S^{0\prime}_{Rxn} = -52$ J/mol·K for the wild-type cyt *c* couple without rearrangement. Comparison of these entropies indicates that the oxidized $His_{82}$-$Fe^{3+}$-$His_{18}$ form is highly disordered. It is proposed that this high level of disorder facilitates rapid rearrangement to $Met_{80}$-$Fe^{2+}$-$His_{18}$ upon reduction.

Axial coordination of the heme iron plays a major role in determining the redox, electron transfer, and other properties of cytochrome *c* (cyt *c*)[1] and other heme proteins (*1*−*3*). While methionine and histidine are invariably the axial ligands of wild-type mitochondrial cyt *c*, other variants have these ligands substituted or deleted (*1*, *4*). Closely allied to changes in axial coordination and of significant interest are pH (native versus alkaline form) (*5*, *6*) and redox (folded versus unfolded form) "switched" changes in axial coordination (*7*, *8*). Recently, heme ligand switching has been observed during catalysis in the cytochromes of cytochrome $cd_1$ nitrite reductase, which catalyzes the conversion of nitrite to nitric oxide in the nitrogen cycle (*9*). In the oxidized enzyme the $d_1$ heme iron of the active site is coordinated by His/Tyr side chains, and the *c* heme is coordinated by a pair of His/His ligands. Upon reduction of the oxidized crystals, it was found (*9*) that the tyrosine ligand of the $d_1$ heme was released to allow substrate binding. Concomitantly, a refolding of the cyt *c* was observed which resulted in an unexpected change in the *c* heme iron coordination from His17/His69 to Met106/His69. While it was suggested that the equilibrium reduction potentials must change for these

[†] This work was supported by the National Institutes of Health Grant GM 48598 to B.A.F., National Institutes of Health Grant GM 55917 to M.D.R., and a grant to E.M. from the Edward Mallinckrodt, Jr., Foundation.

* To whom correspondence should be addressed: B.A.F. (tel, 414 229-4169; fax, 414 229-5530; e-mail, feinberg@csd.uwm.edu) or M.D.R. (tel, 414 288-1625; fax, 414 288-7066; e-mail, ryanm@marquette.edu).

[§] University of Wisconsin−Milwaukee.

[‖] University of Illinois at Chicago.

[‡] Marquette University.

[⊥] Tel-Aviv University.

[1] Abbreviations: Ag/AgCl, silver/silver chloride reference electrode; BPD, bis(4-pyridyl) disulfide; CV, cyclic voltammetry; Cys102Ser, cysteine-102-serine; cyt *c*, cytochrome *c*; $E_s$, step potential; $E_{sw}$, square-wave amplitude; Phe82His, phenylalanine-82-histidine; s, second; SHE, standard hydrogen electrode; SWV, square-wave voltammetry; SW, square-wave.

S0006-2960(98)01037-X CCC: $15.00 
Published on Web 08/29/1998

two forms, they were not determined. Likely changes in reduction potential were interpreted as a mechanism for gating electron flow in this "multielectron" enzyme. Williams et al. (*9*) also showed that after the nitric oxide was formed and expelled from the active site, both hemes returned to their starting coordination. These coordination changes and rearrangements were seen as a mechanism for converting redox energy into "conformational" energy. Last, similar events occur for the refolding of mitochondrial cyt *c*, when the protein switches from an intermediate His/His coordinated form to the native Met/His form (*10*−*13*).

In this paper we explore the unusual redox driven behavior of the Phe82His mutant of yeast iso-1-cyt *c*. This mutant also carries a Cys102Ser change to prevent disulfide dimerization of the protein (*14*, *15*), which may alter the cytochrome's thermodynamic and spectroscopic parameters. Throughout this paper this double mutant is referred to as the Phe82His variant. In considering redox switched and controlled coordination, it has long been proposed for cyt *c* that the coordination bond of the Met80 sulfur to the ferrous ($Fe^{2+}$) heme is a particularly strong one (*16*, *17*). In contrast, the Met80−$Fe^{3+}$ bond is weaker, and ligands such as imidazole and cyanide can displace the protein Met80 ligand in the oxidized state (*18*).

In an earlier study of this novel Phe82His variant of iso-1-cyt *c*, EPR and optical spectroscopies of the oxidized protein (*19*) indicated that the replacement of Phe82 by histidine resulted in bis-imidazole coordination of the oxidized heme iron. Met80 was apparently replaced by the new His82 as the sixth axial ligand, even though (*19*) the original two coordinating ligands of the heme (Met80 and His18) were not varied. In a subsequent study of this variant (*20*), it was found that when the protein was reduced with dithionite and maintained rigorously anaerobic, the $^1$H NMR spectrum showed the peaks of the coordinated Met80 sidechain protons at positions and with intensities nearly identical to those previously assigned for both the wild-type protein and the Cys102 mutants (*14*, *21*). Together, these studies imply that the Phe82His variant undergoes an oxidation-state triggered intramolecular rearrangement with changes in axial coordination.

Work presented here extends our knowledge of redox driven intramolecular "switched" rearrangements. It also demonstrates the likely importance of differences in ferrous and ferric coordination by showing that the Met80−$Fe^{2+}$ bond not only may provide significant stability for native cyt *c* but may also facilitate the reformation of the wild-type form of the reduced state of the Phe82His variant. We show with the dynamic electrochemical methods of cyclic and square-wave voltammetry that the Phe82His variant undergoes a redox driven and reversible rearrangement between two coordinated forms: $Met_{80}$-$Fe^{2+}$-$His_{18}$ and $His_{82}$-$Fe^{3+}$-$His_{18}$. Since these are dynamic electron-transfer/rearrangement events, the methods of voltammetry are ideally suited for their direct observation and interpretation. For the first time, a detailed 2 × 2 electrochemical mechanism is presented for a redox protein that undergoes redox driven rearrangement. Other key questions to be addressed are: (1) What is the net redox reaction of this variant and its thermodynamic equilibrium reduction potential? (2) What are the thermodynamic equilibrium reduction potentials for the participating coordinated forms? (3) What are the rate constants for intramolecular rearrangement? (4) To what extent are these forms in equilibrium within a given redox state? (5) What are the entropic contributions to the electron-transfer reaction itself, and how do they contribute to the redox-dependent/redox-switched intramolecular rearrangement?

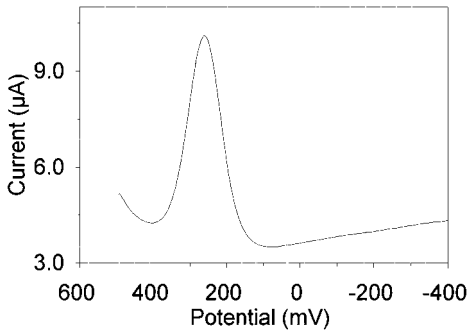


FIGURE 1: Square-wave voltammogram of 1.0 mM Cys102Ser mutant of yeast iso-cyt *c* at pH 7.0 Tris buffer, 100 mM NaCl. Negative scan from $E_i = +500$ mV to $E_f = -400$ mV, $E_{sw} = 25$ mV, $f = 15$ Hz, and $E_s = 4$ mV with a 2-s holding time before starting scan. Potentials are versus SHE.

## EXPERIMENTAL METHODS

### *Electrochemical Methods*

*(1) Square-Wave Voltammetry.* Square-wave voltammetry (SWV) is an electrochemical method which provides a high signal-to-noise response (*22*). Osteryoung and co-workers have been largely responsible for developing square-wave voltammetry and making it accessible (*23*, *24*). SWV is significantly more sensitive than cyclic voltammetry (CV) (*23*). Recently, SWV has been applied to the study of the iron−sulfur proteins and enzymes (*25*−*28*). In SWV a potential is applied over time in the form of a square-wave superimposed on a staircase (*28*). The applied potential is progressively stepped in fixed increments, $E_s$ (the step potential), and pulsed positively and negatively at each step with potential $E_{sw}$, the square-wave amplitude. This is done at a particular frequency, $f = \tau^{-1}$, where $\tau$ is the time for one full cycle. The resultant current is measured at the end of each negative and positive pulse. The voltammetric scan is in either the positive or negative direction. For each applied $E_s$, the difference in current is calculated between the positive and negative currents generated from the applied potential pulses. Experimentally, the positive and negative currents are collected separately, and then the differences are taken for all pulses to provide the observed "net" SW voltammogram (see Figure 1). When there are no kinetic complications, the potential at which the voltammetric peak is observed defines the equilibrium reduction potential, $E^{0\prime}$. The width at half-height, $W_{1/2}$, is a measure of reversibility; the redox reaction is reversible when $W_{1/2} = 90/n$ mV, with $n$ being the number of electrons transferred. The height of a SW voltammetric peak is proportional to the relative concentration of the particular species that the peak represents. All events occur in a thin reaction layer at the electrode surface. SWV experiments done in this work were shown to be diffusion-controlled, since the peak current, $i_p$, versus $\tau^{-1/2}$ was linear (data not shown).

*(2) Cyclic Voltammetry.* While CV is not as sensitive as SWV in the present case, it has some important advantages

and provides for (1) the direct observation of the two forms/redox couples and the relative contributions of the reducing/oxidizing current to each couple and (2) a fundamentally more direct and obvious interpretation of the voltammograms, especially as a function of scan rate. In CV the potential waveform applied to the electrode is a simple triangular wave in which the potential is first scanned in one direction and then, at some point, switched and scanned in the reverse direction. For example, when the potential is scanned in the positive direction, the reduced redox center is oxidized as the potential approaches and goes past the $E^{0\prime}$ of that species, and then upon scanning the potential in the reverse (negative) direction, the redox center is reduced again. A single-scan CV, thus, gives a pair of peaks of the same current amplitude with the $E^{0\prime}$ between them and separated by 60 mV/*n*, if the redox reaction is fast and reversible. The CV experiments were also shown to be diffusion-controlled, since $i_p$ versus (scan rate)$^{1/2}$ was linear (data not shown). All cyclic voltammograms are uncorrected for background current; nonetheless, the simulated and observed cyclic voltammograms of the Phe82His variant at each scan rate are very similar (see Discussion).

*Simulation of Cyclic Voltammograms and Kinetic Rate Constants.* A new and very fast method for simulating cyclic voltammograms has been developed (*29*−*31*) which permits the determination of the rates of production of new products, intermediates, and equilibrium constants in the context of a specific mechanism and as a function of scan rate. This method has now been formalized in the computer software Digisim (Bioanalytical Systems, Lafayette, IN), which is used in this work. If a series of voltammograms at different scan rates are all well-simulated with a single set of kinetic rates and equilibrium constants for a specific mechanism, then the simulations provide strong supportive evidence for the mechanism and for the validity of those rates and equilibrium constants.

*Instrumentation.* All electrochemical experiments were done with a BAS 100 B/W electrochemical analyzer (Bioanalytical Systems). Potentials are reported against either the standard hydrogen electrode (SHE) or the Ag/AgCl/3 M KCl reference electrode. To convert the Ag/AgCl potentials shown for all the cyclic voltammograms to the SHE, simply add 199 mV (Ag/AgCl reference) to that potential. The buffer used throughout this work, unless otherwise stated, was 50 mM Tris, 100 mM NaCl, pH 7.0. Tris HCl, Tris Base, and NaCl were obtained as ultrapure reagents (J. T. Baker). Triple-distilled water (Purification Systems) with a conductivity of 18 MΩ/cm was used. Final protein concentrations were about 0.5 to 1 mM. Microdialysis (typically of 100-$\mu$L samples) was used to change buffers and/or exogenous ligand concentration. A disk of 3-mm diameter gold electrode (99.999%, Johnson Matthey) was encased in a casting resin sheath as the working electrode. The electrode was polished with 0.3-$\mu$m alumina slurries (Buehler, Lake Bluff, IL) and rinsed with distilled water to remove polishing material and further clean the electrode surface. After the gold electrode surface was polished, it was modified by dipping it in a fresh 5 mM solution of bis(4-pyridyl) disulfide (BPD) (Aldrich Chemical Co.) promoter for 10 min. The BPD promoter facilitates electron transfer between the cyt *c* and the electrode surface but is not electrochemically active itself. The electrode was then washed with distilled water and used immediately. The BPD-modified gold electrode (*32*) has been used previously (*33*) to study similar cytochromes *c*.

A specially designed anaerobic semimicrocell that permits samples of about 30-$\mu$L volume to be examined was used for the electrochemical experiments (*25, 26*). The small volume of sample is effectively maintained between the working, reference, and auxiliary electrodes. Oxygen was removed by passing wet 99.99% pure nitrogen over the sample and through the cell for 20 min prior to the experiment. The reference electrode used was an Ag/AgCl/3 M KCl electrode. The counter electrode was 18-gauge platinum wire.

*Entropic Contributions to the Reduction Potential of the Cytochromes c by Nonisothermal Electrochemistry.* A water jacked semimicrocell, similar to that described above, permitted rapid and precise control of the temperature of the cyt *c* sample for nonisothermal electrochemical experiments. The advantage of nonisothermal electrochemical measurements of the reduction potential, $E^{0\prime}$, as a function of temperature is that the slope of $E^{0\prime}$ versus $T$ is directly proportional to the entropy of reaction: $\Delta S^{0\prime}_{Rxn}$ (*34*). In these experiments, only the sample changes temperature, while the temperature of the reference electrode is kept constant. A Ag/AgCl reference electrode was prepared with a 1-mm diameter, 8-cm length of anodized silver wire in an electrode assembly 25 cm long. In this arrangement the reference electrode at the top of the assembly remained at constant room temperature for the duration of the experiment. Only the bottom 1.5 cm of the electrode assembly, with a porous Vycor glass tip, was in the temperature-controlled cell and made contact with the cyt *c* solution, which was brought to equilibrium at each new temperature where the $E^{0\prime}$ was determined by SWV. The thermal junction potentials were evaluated experimentally, and the observed redox potentials were determined to be within ±0.3 mV of their true values over the temperature range from 2 to 40 °C. The experimental data of the WT and variant cyt *c* were obtained in the range of 4−37 °C. In the nonisothermal experiment, the electron-transfer reaction evaluated is the reduction of the cyt *c*, with one electron transferred ($n = 1$):

$$\text{cyt } c\ (Fe^{3+}) + e^- \rightleftarrows \text{cyt } c\ (Fe^{2+}) \qquad (1)$$

In the expression:

$$\Delta G^{0\prime} = -nFE^{0\prime} = \Delta H^{0\prime} - T\Delta S^{0\prime} \qquad (2)$$

$\Delta G^{0\prime}$ is the free energy for the reduction process, $\Delta H^{0\prime}$ and $\Delta S^{0\prime}$ are the enthalpic and entropic components of $\Delta G^{0\prime}$, $n$ is the number of electrons transferred, and $F$ is the Faraday constant in coulomb/mol. Moreover,

$$d\Delta G^{0\prime}/dT = -nF(dE^{0\prime}/dT) = \Delta S^{0\prime}_{Rxn} \qquad (3)$$

where $\Delta S^{0\prime}_{Rxn}$ is the observed entropy of reaction. Furthermore, $\Delta S^{0\prime}_{Rxn}$ is also the difference between the individual standard entropies of the reduced and oxidized states of the protein:

$$\Delta S^{0\prime}_{Rxn} = S^{0\prime}_{Red} - S^{0\prime}_{Ox} = S^{0\prime}_{Cyt,Fe^{2+}} - S^{0\prime}_{Cyt,Fe^{3+}} \qquad (4)$$

Following recommended practice (*35*), the standard entropy

change, $\Delta S^{0\prime}$, at 25 °C, was equated to the practical entropy scale and calculated as:

$$\Delta S^{0\prime} = \Delta S^{0\prime}_{\mathrm{Rxn}} - 66.5\ \mathrm{J/mol{\cdot}K} \qquad (5)$$

Since $\Delta G^{0\prime} = -nFE^{0\prime}$, $\Delta G^{0\prime}_{\mathrm{Obs}}$ is calculated from the observed reduction potential of the cytochrome; $\Delta H^{0\prime}$ is then obtained from $\Delta S^{0\prime}$ and $\Delta G^{0\prime}$. For discussions of entropic contributions to the reduction potentials of cytochromes, see Bertrand et al. (*36*) and Taniguchi et al. (*35*).

*Preparation of the Cys102Ser and Phe82His/Cys102Ser Iso-1-cytochromes c.* All DNA manipulations were carried out according to the procedures described by Maniatis et al. (*37*). Oligonucleotides were purchased from Operon. Enzymes (restriction enzymes, ligase, and *Pfu* DNA polymerase) were purchased from Promega, Boehringer Mannheim, or Stratagene and used according to the manufacturers' recommendations. Media components used in the growth of *Escherichia coli* and yeast cells were purchased from Difco and antibiotics from Sigma Chemical Co. All other chemicals were obtained from Fisher or Sigma.

The yeast *E. coli* shuttle vector YEpCYC1 has been described previously (*38*). Bacterial strain DH5α was used to manipulate DNA. Yeast strain GM-3C-2 (α, leu2,-3, leu2-112, trp1-1, his4-519, cyc1-1, cyp3-1), which has no functional endogenous cyt *c* genes, was used to express the recombinant cyt *c* genes (*39*). The site-directed mutagenesis of cyt *c* genes by PCR was performed as described previously (*40*). Plasmid YEp*CYC1-C102S*, which contained the yeast iso-1-cyt *c* gene *CYC1* with cysteine at 102 being replaced by serine, was used as the template for the PCR reaction for the C102S-F82H double mutant. The accuracy of the mutant construct was verified by DNA sequencing. The construction of yeast expression vector YEp*CYC1*, transformation of yeast strain GM-3C-2, large-scale fermentation of the transformed yeast, and purification of the mutant cyt *c* proteins were carried out as described earlier (*38*). HPLC fraction II, the N-terminal nonacetylated cyt *c*, was used exclusively.

## RESULTS

*Yield of the Phe82His/Cys102Ser Mutant Cytochrome c*. The wet cell pellets weighed about 2 kg, an amount similar to that obtained with the same fermentation employing the same yeast strain carrying a wild-type cyt *c* gene. However, the yield of this mutant was over 400 mg/kg of wet yeast paste, while that of the wild-type as well as a number of other cyt *c* mutants is no more than 50−100 mg/kg. This is the first time we have observed such a dramatic increase in the amount of recombinant cyt *c* prepared in our system.

Since wild-type yeast iso-1-cyt *c* has a free cysteine at position 102 which can complicate experiments through dimerization and autoreduction, Cys102Thr or Cys102Ser mutants are prepared to eliminate these problems. It has been shown that Ser or Thr mutation at the Cys102 position does not significantly alter the properties of the protein (*14, 21, 41*). Thus, the Cys102Thr variant is referred to throughout this paper as the wild-type cyt *c*.

*Square-Wave Voltammetry of the Wild-Type and the Phe82His Variant.* Figure 1 shows the SWV of the wild-type cyt *c* with an observed $E^{0\prime} = +269$ mV, a value identical to that reported for native yeast iso-1-cyt *c* at pH 7 (*41*). Figure 2 shows the SWV of the Phe82His variant. In Figure 2a the voltammetry experiment is begun at the reducing potential of −400 mV, held for 2 s, and then scanned in the positive direction. Upon scanning in the positive direction, two electrochemically distinct species were observed: a small voltammetric peak at $E^{0\prime} \simeq -148$ mV and a significantly larger (higher current) peak at $E^{0\prime} \simeq +229$ mV. Next, and without changing the sample or cell configuration, the reverse experiment was done (see Figure 2b) in which the potential was held at the oxidizing potential of +500 mV for 2 s and was followed by a voltammetric scan in the negative or reducing direction. While the same two voltammetric peaks were observed, their relative peak heights were reversed. Using the same sample, these steps were done repeatedly, demonstrating that the redox potential drives and controls which form predominates. Tentative assignments for these redox couples are the $Met_{80}$-$Fe^{3+/2+}$-$His_{18}$ redox couple at $E^{0\prime} \simeq +229$ mV and the $His_{82}$-$Fe^{3+/2+}$-$His_{18}$ redox couple at $E^{0\prime} \simeq -148$ mV.

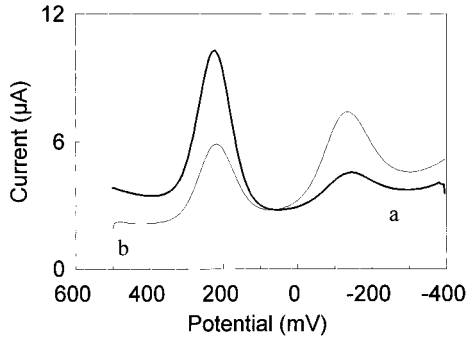


FIGURE 2: Square-wave voltammetry of 1.0 mM Phe82His/Cys102Ser mutant of iso-cyt *c* at pH 7.0 Tris buffer, 100 mM NaCl. (a) Positive scan from $E_i = -400$ mV to $E_f = +500$ mV, $E_{sw} = 25$ mV, $f = 15$ Hz, and $E_s = 4$ mV with 2-s holding time before starting scan. (b) Negative scan from $E_i = +500$ mV to $E_f = -400$ mV, $E_{sw} = 25$ mV, $f = 15$ Hz, and $E_s = 4$ mV with 2-s holding time before starting scan. Potentials are versus SHE.

*Square-Wave Voltammetry of the Wild-Type Cytochrome c in the Presence of Imidazole.* To make a definite assignment of the voltammetric peak observed above for the $E^{0\prime} \simeq -148$ mV species, the electrochemistry of the wild-type cyt *c* was examined in the presence of imidazole. It is well-established (*18*) that in the oxidized state exogenous imidazole coordinates to the $Fe^{3+}$. SW voltammetry was carried out for the wild-type cyt *c* in the presence of 100 mM imidazole (see Figure 3). In Figure 3a, the potential scan was begun at −400 mV and scanned in the positive direction. The native $Met_{80}$-Fe-$His_{18}$ form predominated, but a substantial portion of it remained in a new low potential form at $E^{0\prime} \simeq -126$ mV. This clearly corresponds to the $Imid_{exogenous}$-$Fe^{3+}$-$His_{18}$ form. When the scan is started from a positive potential (Figure 3b) and scanned in the negative direction, the $Imid_{exogenous}$-$Fe^{3+}$-$His_{18}$ form predominates, since its formation is favored when the protein is in the oxidized state (*18*).

*Cyclic Voltammetry of the Phe82His Variant.* Figure 4 shows the cyclic voltammogram of the Phe82His iso-1-cyt *c* at a moderate scan rate of 50 mV/s. The same two redox couples were observed with essentially the same reduction potentials as obtained from SWV in Figure 2, but the couple at the relatively negative potential has little or no reverse current; i.e., it appears to be nearly irreversible. The potentials for this and other CVs are shown versus the Ag/

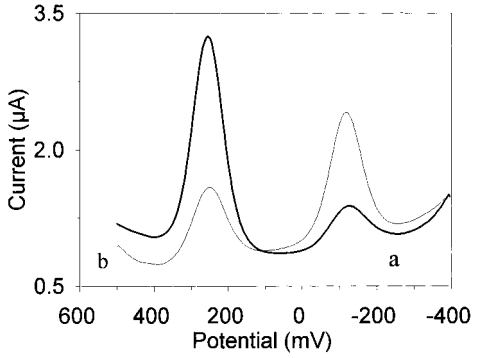


FIGURE 3: Square-wave voltammetry of 1.0 mM Cys102Ser mutant of iso-cyt *c* at pH 7.0 Tris buffer, 100 mM NaCl, 100 mM imidazole. (a) Positive scan from $E_i = -400$ mV to $E_f = +500$ mV, $E_{sw} = 25$ mV, $f = 15$ Hz, and $E_s = 4$ mV with 2-s holding time before starting scan. (b) Negative from $E_i = +500$ mV to $E_f = -400$ mV, $E_{sw} = 25$ mV, $f = 15$ Hz, and $E_s = 4$ mV with 2-s holding time before starting scan. Potentials are versus SHE.

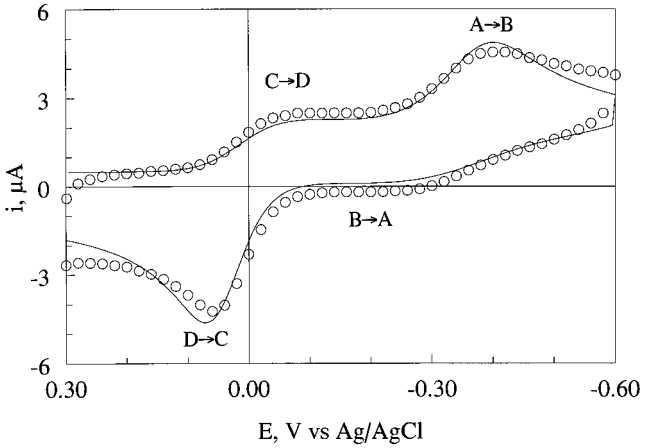


FIGURE 4: Cyclic voltammetry and its associated simulation for the Phe82His/Cys102Ser start voltammogram with negative scan from $E_i = +500$ mV to $E_{switch} = -400$ mV and return to $E_i = +500$ mV; scan rate 50 mV/s. The data points are circles (○), and the simulation is the solid line. Potentials are versus Ag/AgCl. Assuming that $E^{0\prime}_{AB} \simeq 47$ mV vs SHE (or $-152$ vs Ag/AgCl), then from eq 14, $K_{BD} = 3.6 \times 10^5$ s$^{-1}$ was calculated, and from the scan rate, $k_{f,BD} > 10$ s$^{-1}$ was approximated.

AgCl reference electrode. To obtain the potential vs SHE, add 199 mV.

*Simulations of the Observed Cyclic Voltammograms at Different Scan Rates.* Shown in Figure 4 is the cyclic voltammogram done at 50 mV/s scan rate with the simulated cyclic (solid line) voltammogram superimposed upon the experimental cyclic voltammogram (circles). For this and other simulations of the voltammetric experiments at different scan rates, the 2 × 2 mechanism was adopted (see Scheme 1) together with well-chosen "starting" thermodynamic equilibrium $E^{0\prime}$ values for the $His_{82}$-$Fe^{2+/3+}$-$His_{18}$ and $Met_{80}$-$Fe^{2+/3+}$-$His_{18}$ redox couples. The cyclic voltammograms, with their associated simulations, for the Phe82His iso-1-cyt *c* at three different scan rates (10, 100, and 500 mV/s) are shown in Figure 5. For each voltammogram, the scan was begun at the positive potential of +300 mV vs Ag/AgCl (500 mV vs SHE) and scanned negatively to −600 mV vs Ag/AgCl and then back to +300 mV at the different scan rates. The simulation of the observed cyclic voltammograms provided values for the thermodynamic equilibrium $E^{0\prime}$ values for all forms and relative values for their equilibrium

Scheme 1: Proposed 2 × 2 Mechanism for Redox Driven Rearrangement and Ligand Exchange

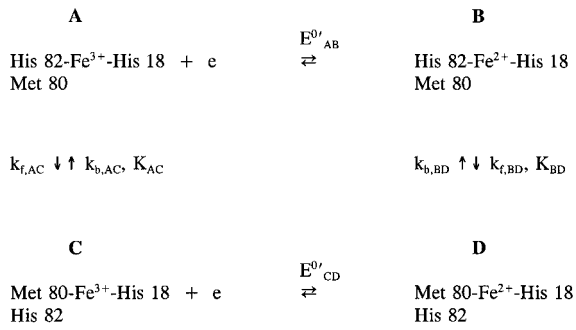


Where: $K_{AC}$ = [Met 80-$Fe^{3+}$-His 18]/[His 82-$Fe^{3+}$-His 18] < 1
$K_{BD}$ = [Met 80-$Fe^{2+}$-His 18]/[His 82-$Fe^{2+}$-His 18] > 1

constants and rates of ligand exchange/molecular rearrangement (see Discussion).

*Nonisothermal Determination of the Entropy of Reaction,* $\Delta S^{0\prime}_{Rxn}$. Using the cell/electrode assembly described above, square-wave voltammetric nonisothermal determinations of the entropy of reaction, $\Delta S^{0\prime}_{Rxn}$, were first made for purified horse heart cyt *c*, since this is the first time that SWV has been used to make these measurements. The entropy of reaction obtained for horse heart cyt *c*, −48 J/mol·K, was in excellent agreement with values obtained previously at similar ionic strengths and obtained both electrochemically and calorimetrically (see Table 1). The entropies of reaction and associated thermodynamic values were also determined for the wild-type iso-1-cyt *c* (in the absence and presence of imidazole) and its Phe82His variant. For the Phe82His variant the net redox couple evaluated was necessarily the cross-reaction: $His_{82}$-$Fe^{3+}$-$His_{18}$ + $e^-$ → $Met_{80}$-$Fe^{2+}$-$His_{18}$ (see Discussion). To determine this $\Delta S^{0\prime}_{Rxn}$ (−80 J/mol·K), the $E^{0\prime}$ of the quasi-reversible couple at +229 mV was followed as a function of temperature. All experimental $E^{0\prime}$ vs *T* plots over the temperature range of 4−37 °C were linear and were done at least four times (data not shown). SWV peak currents changed only slightly with temperature as expected, with no large current decrements, thus indicating that no denaturation of either wild-type or variant cyt *c* occurred. For the wild-type cyt *c*, the net redox couple evaluated was $Met_{80}$-$Fe^{3+}$-$His_{18}$ + $e^-$ → $Met_{80}$-$Fe^{2+}$-$His_{18}$ ($\Delta S^{0\prime}_{Rxn} = -52$ J/mol·K). These results are summarized in Table 2.

## DISCUSSION

*Square-Wave Voltammetry of the Wild-Type and Phe82His Variant of Iso-1-cytochrome c.* In the square-wave voltammetry of the Phe82His variant, the $E^{0\prime} \simeq +229$ mV species is assigned to the $Met_{80}$-$Fe^{2+/3+}$-$His_{18}$ redox couple of iso-1-cyt *c*. Thus, the reduction potential is shifted from $E^{0\prime} \simeq +269$ mV for the wild-type to $E^{0\prime} \simeq +229$ mV for the Phe82His variant. This latter reduction potential is similar to those determined for other iso-1-cyt *c* Phe82 mutants which have their $E^{0\prime}$ values lowered by 10−42 mV (*42*). Generally, mutations at Phe82 lead to a destabilized, more open oxidized form, which, in turn, typically lowers the reduction potential (*43*). We will show later that the $E^{0\prime}$ of the $His_{82}$-$Fe^{2+/3+}$-$His_{18}$ couple is also necessarily shifted to a more negative potential by virtue of its subsequent redox

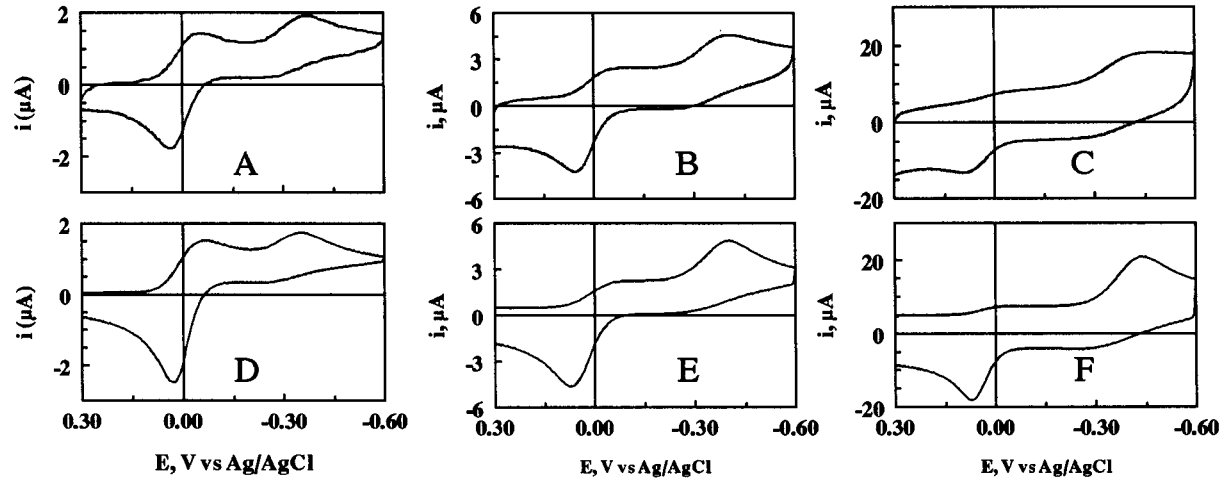


FIGURE 5: Experimental/digitally simulated cyclic voltammograms of the Phe82His/Cys102Ser variant at three different scan rates: A/D, 10 mV/s; B/E, 100 mV/s; and C/F, 500 mV/s. Potentials are versus Ag/AgCl. Assuming that $E^{0\prime}_{AB} \simeq 47$ mV vs SHE (or $-152$ vs Ag/AgCl), then from eq 14, $K_{BD} = 3.6 \times 10^5$ s$^{-1}$ was calculated, and from the scan rate, $k_{f,BD} > 10$ s$^{-1}$ was approximated.

Table 1: Comparison of Square-Wave Voltammetric Determination of $\Delta S^{0\prime}_{Rxn}$ for Horse Cytochrome *c* at 25 °C, pH 7 with Earlier Determinations

| source | $\Delta S^{0\prime}_{Rxn}$, J/mol·K (cal/mol·K) | $T\Delta S^{0\prime}$, kJ/mol (kcal/mol) | $\Delta H^{0\prime}$, kJ/mol (kcal/mol) | *I*, M |
|---|---|---|---|---|
| this work | $-48 \pm 3$ ($-11.5$) | $-34 \pm 1$ ($-8.1$) | $-58 \pm 1$ ($-13.9$) | 0.123 |
| ref *36* | $-53 \pm 8$ ($-12.7$) | $-36 \pm 3$ ($-8.6$) | $-60 \pm 3$ ($-14.3$) | 0.10 |
| ref *52* | $-48 \pm 2$ ($-11.7$) | $-34 \pm 1$ ($-8.1$) | $-59 \pm 2$ ($-14.1$) | 0.13 |
| ref *35* | $-62 \pm 5$ ($-14.9$) | $-38 \pm 2$ ($-9.1$) | $-64 \pm 2$ ($-15.2$) | 0.10 |

driven rearrangement in the 2 × 2 mechanism: $His_{82}$-$Fe^{3+}$-$His_{18}$ + $e^- \rightarrow$ $Met_{80}$-$Fe^{2+}$-$His_{18}$.

The $E^{0\prime} \simeq -148$ mV species is assigned to the $His_{82}$-$Fe^{3+/2+}$-$His_{18}$ redox couple. Previous work suggests that the $E^{0\prime}$ values for cyt *c* imidazole-$Fe^{2+/3+}$-His forms are quite negative compared to the native cyt *c* reduction potential (*44*). When the electrode potential was initially held at a positive potential and scanned in the negative direction, the $E^{0\prime} \simeq -148$ mV species predominated (higher peak current) over the $Met_{80}$-Fe−$His_{18}$ form at $E^{0\prime} \simeq +229$ mV species (see Figure 2a). Conversely, the $Met_{80}$-Fe−$His_{18}$ form predominated when the electrode potential was initially poised at a negative (reducing) potential and then scanned in the positive direction (see Figure 2b). These experiments were repeated by cycling back and forth at either a positive or a negative applied potential to drive and shift the relative amounts of each form as a function of redox state. These results show explicitly that the Phe82His variant undergoes reversible and fast changes in axial coordination, in which the equilibrium distribution of each form is shifted toward the $His_{82}$-Fe-$His_{18}$ or $Met_{80}$-Fe-$His_{18}$ form, depending on the initial applied potential. Furthermore, since Phe82 resides in a different spatial position than the native Met80, the protein necessarily has to intramolecularly rearrange for the His82 to coordinate to the $Fe^{3+}$ heme. It rearranges again upon reduction, when the Met80 displaces the His82 and coordinates to the $Fe^{2+}$ heme. Under the electrochemical conditions described here, however, at no time was 100% of either form observed. This is partly due to the equilibrium between $His_{82}$-$Fe^{3+}$-$His_{18}$ and $Met_{80}$-$Fe^{3+}$-$His_{18}$ discussed below.

*Square-Wave Voltammetry of the Wild-Type Cytochrome in the Presence of Imidazole.* The square-wave voltammetric examination of the wild-type cyt *c* in the presence of imidazole is shown in Figure 3 and serves to mimic the behavior of the Phe82His variant. It is well-established that, in the oxidized state, cyt *c* coordinates strongly with imidazole or cyanide ions (*17*), but upon reduction Met80 displaces these species to attain the native $Met_{80}$-$Fe^{2+}$-$His_{18}$ form. The experiments shown in Figure 3 confirm this behavior. It has also been shown that when Met80 is substituted with *exogenous* imidazole, the redox potential is dramatically lowered, e.g., for horse cyt *c* the $E^{0\prime} = -178$ mV vs +262 mV for the wild-type protein (*44*, *45*). The redox behavior of the wild-type iso-1 cyt *c* complex with imidazole is remarkably similar to that of the Phe82His variant and provides additional evidence that for this variant, the low-potential species at $E^{0\prime} \simeq -148$ mV is, indeed, the $His_{82}$-$Fe^{3+/2+}$-$His_{18}$ form as previously concluded (*19*). The wild-type cyt *c* without imidazole (Figure 1) has only one voltammetric peak within the range of +500 to −600 mV vs SHE and no additional observable electrochemistry.

*Cyclic Voltammetry and Assignment of Redox Couples.* The identification and assignment of the redox couples in the cyclic voltammetric experiments follow lines similar to

Table 2: Reduction Potentials, Entropies of Reaction, and Entropic and Enthalpic Contributions to the $E^{0\prime}$ of Wild-Type and Phe82His Iso-1-cytochromes *c*

| cyt *c* | $E^{0\prime}$, mV (kcal/mol) | $\Delta S^{0\prime}_{Rxn}$, J/mol·K (cal/mol·K) | $T\Delta S^{0\prime}$, kJ/mol (kcal/mol) | $\Delta H^{0\prime}$, kJ/mol (kcal/mol) |
|---|---|---|---|---|
| Cys102Ser[a] | +269 (−6.2) | $-52 \pm 2$ ($-12.4$) | $-35 \pm 1$ ($-8.4$) | $-61 \pm 1$ ($-14.6$) |
| Phe82His/Cys102Ser[b] | $+229 \pm 3$ ($-5.3$) | $-80 \pm 2$ ($-19.1$) | $-44 \pm 1$ ($-10.5$) | $-66 \pm 1$ ($-15.8$) |
| Cys102Ser/imidazole[c] | $+255 \pm 2$ | $-97 \pm 1$ ($-23.2$) | $-49 \pm 1$ ($-11.7$) | $-73 \pm 1$ ($-17.4$) |

[a] Net reaction: $Met_{80}$-$Fe^{3+}$-$His_{18}$ + $e^- \rightarrow$ $Met_{80}$-$Fe^{2+}$-$His_{18}$. [b] Net reaction: $His_{82}$-$Fe^{3+}$-$His_{18}$ + $e^- \rightarrow$ $Met_{80}$-$Fe^{2+}$-$His_{18}$. [c] Net reaction: imidazole-$Fe^{3+}$-$His_{18}$ + $e^- \rightarrow$ $Met_{80}$-$Fe^{2+}$-$His_{18}$.

that for square-wave voltammetry. Figure 4 shows a typical cyclic voltammogram of the Phe82His variant at the modestly slow scan rate of 50 mV/s, which graphically illustrates the transformations indicated by square-wave voltammetry. When starting at the very positive potential of 300 mV vs Ag/AgCl (+500 mV vs SHE) the cyt *c* ($E^{0\prime} \simeq +229$ mV) is fully oxidized and presumably in the $His_{82}$-$Fe^{3+}$-$His_{18}$ form. Nonetheless, as the potential is scanned in the negative direction, peak C → D is observed and assigned to:

peak C → D:

$$\underset{\text{C}}{\text{Met}_{80}\text{-Fe}^{3+}\text{-His}_{18}} + e^- \rightarrow \underset{\text{D}}{\text{Met}_{80}\text{-Fe}^{2+}\text{-His}_{18}} \quad (6)$$

As seen in Figure 5, for both the observed and simulated voltammograms, this peak *decreases* in current magnitude as the scan rate increases. The reason for this is that at slow scan rates, the predominant $His_{82}$-$Fe^{3+}$-$His_{18}$ form at oxidizing potentials undergoes the following equilibrium reaction (see Scheme 1) to produce the $Met_{80}$-$Fe^{3+}$-$His_{18}$ form, which is then reduced and seen as C → D:

$$\underset{\text{Met}_{80}}{\text{His}_{82}\text{-Fe}^{3+}\text{-His}_{18}} \underset{k_{\text{b,AC}}}{\overset{k_{\text{f,AC}}}{\rightleftharpoons}} \underset{\text{His}_{82}}{\text{Met}_{80}\text{-Fe}^{3+}\text{-His}_{18}} \quad (7)$$
$$\text{A} \qquad\qquad \text{C}$$

At slow scan rates, as the $Met_{80}$-$Fe^{3+}$-$His_{18}$ form is reduced to $Met_{80}$-$Fe^{2+}$-$His_{18}$, $Met_{80}$-$Fe^{3+}$-$His_{18}$ is replenished through this equilibrium process. At higher scan rates, not enough time is permitted for the equilibrium to replenish $Met_{80}$-$Fe^{3+}$-$His_{18}$, and the relative current seen for the reduction of this form decreases as the scan rate increases. Thus, by using faster scan rates we have "caught up" with the equilibrium process.

As the scan is continued in the negative direction, the predominant $His_{82}$-$Fe^{3+}$-$His_{18}$ form is reduced and seen as the A → B peak, which provides a relatively large reduction current:

peak A → B:

$$\underset{\text{A}}{\text{His}_{82}\text{-Fe}^{3+}\text{-His}_{18}} + e^- \rightarrow \underset{\text{B}}{\text{His}_{82}\text{-Fe}^{2+}\text{-His}_{18}} \quad (8)$$

At −600 mV vs Ag/AgCl the direction of the potential scan is reversed, and the potential is now scanned in the positive direction. As the scan is continued in the positive direction, essentially *no current*/*peak* is seen for the reoxidation B to A, i.e., B → A:

peak B → A:

$$\underset{\text{B}}{\text{His}_{82}\text{-Fe}^{2+}\text{-His}_{18}} - e^- \rightarrow \underset{\text{A}}{\text{His}_{82}\text{-Fe}^{3+}\text{-His}_{18}} \quad (9)$$

The reason for this is that $His_{82}$-$Fe^{2+}$-$His_{18}$ form (B) is transient. Immediately after its formation (peak A → B), it rapidly interconverts to the $Met_{80}$-$Fe^{2+}$-$His_{18}$ form through ligand exchange/protein rearrangement:

$$\underset{\text{Met}_{80}}{\text{His}_{82}\text{-Fe}^{2+}\text{-His}_{18}} \xrightarrow{k_{\text{f,BD}}} \underset{\text{His}_{82}}{\text{Met}_{80}\text{-Fe}^{2+}\text{-His}_{18}} \quad (10)$$
$$\text{B} \qquad\qquad \text{D}$$

Since no current was seen for B → A, it appears that on the time scale of the cyclic voltammetric experiment, $k_{\text{f,BD}}$ is a relatively fast reaction. It is fast enough that even at 500 mV/s, we are not able to "catch up" with $k_{\text{f,BD}}$. If the scan rate was fast enough to "catch up" with $k_{\text{f,BD}}$, we would eventually expect to see some B → A. As the potential scan is continued in the positive direction, the product of the above ligand exchange, the $Met_{80}$-$Fe^{2+}$-$His_{18}$ form, is now oxidized to $Met_{80}$-$Fe^{3+}$-$His_{18}$ and produces a relatively large peak current seen as peak D → C:

peak D → C:

$$\underset{\text{His}_{82}}{\text{Met}_{80}\text{-Fe}^{2+}\text{-His}_{18}} - e^- \rightarrow \underset{\text{His}_{82}}{\text{Met}_{80}\text{-Fe}^{3+}\text{-His}_{18}} \quad (11)$$
$$\text{D} \qquad\qquad \text{C}$$

At this point, the entire cycle begins again for the voltammetric experiment, with C rearranging predominantly to A:

$$\underset{\text{His}_{82}}{\text{Met}_{80}\text{-Fe}^{3+}\text{-His}_{18}} \xrightarrow{k_{\text{b,AC}}} \underset{\text{Met}_{80}}{\text{His}_{82}\text{-Fe}^{3+}\text{-His}_{18}} \quad (12)$$
$$\text{C} \qquad\qquad \text{A}$$

In summary, the two redox couples that make up the complete voltammogram are the $Met_{80}$-$Fe^{3+/2+}$-$His_{18}$ redox couple (C/D) with $E^{0\prime} \simeq +229$ mV and the $His_{82}$-$Fe^{3+/2+}$-$His_{18}$ redox couple (A/B) with $E^{0\prime} \simeq -149$ mV. Their redox initiated interconversions are represented by $k_{\text{b,AC}}$ and $k_{\text{f,BD}}$.

### *2 × 2 Mechanism for Redox Driven Ligand Exchange and Intramolecular Rearrangement for the Phe82His Variant*

*Apparent Redox Couples and Net Electrochemical Reaction.* The square-wave and cyclic voltammetric experiments described above support the view that for the oxidized and reduced Phe82His variants, the $His_{82}$-$Fe^{3+}$-$His_{18}$ and $Met_{80}$-$Fe^{2+}$-$His_{18}$ forms predominate, respectively. Each redox couple, however, has one labile form which rearranges to a stable form. The experimental data for these interrelated redox reactions and intramolecular rearrangements are best described by the 2 × 2 electrochemical mechanism (*46*, *47*) shown in Scheme 1. In this paper we present for the first time a detailed 2 × 2 mechanistic description and analysis of the redox driven intramolecular rearrangements of a cytochrome. Some important characteristics of this mechanism are (1) it takes into account the rates of interconversion between the different coordination forms and the equilibria between the two forms in each redox state; (2) the two redox couples noted above are only apparent redox couples, since they represent "kinetic waves" and are necessarily shifted from the positions they would have if the system were at thermodynamic equilibrium, i.e., if there were no labile species or intramolecular interconversions; and (3) in contrast to these apparent redox couples, the 2 × 2 mechanism requires that the net redox reaction observed is that for the concomitant redox/ligand exchange reaction that involves the only two stable species:

$$\underset{\text{A}}{\text{His}_{82}\text{-Fe}^{3+}\text{-His}_{18}} + e^- \xrightarrow{k_{\text{f,AD}}} \underset{\text{D}}{\text{Met}_{80}\text{-Fe}^{2+}\text{-His}_{18}} \quad (13)$$

where the redox couple A/D has $E^{0\prime}_{\text{AD}}$.

*Computer Simulation of the Cyclic Voltammetric Data.* In the computer simulation of the cyclic voltammetric experiments at different scan rates and using the 2 × 2 electrochemical mechanism shown in Scheme 1, two key parameters are initially determined by the simulation: $E^{0\prime}_{AD}$ and the product $K_{AC}\sqrt{k_{b,AC}}$. Additionally, to get the best fit for the three scan rates examined, a heterogeneous rate constant of $1.24 \times 10^{-3}$ cm/s was assumed and was simulation consistent (*29*) for the negative and nearly irreversible C/D couple. The simulation starts with a good approximation for $E^{0\prime}_{AD}$, i.e., the positive redox couple at +229 mV vs SHE for the slow 10 mV/s cyclic voltammogram (see Figure 5). Initially, we do not know the values for $E^{0\prime}_{CD}$, $E^{0\prime}_{AB}$, $K_{AC}$, and $K_{BD}$. From the mechanism, however, we know that $K_{AC} < 1$. From the simulation at all three scan rates (also Figure 5) it was determined that $E^{0\prime}_{AD} = 176$ mV vs SHE and $K_{AC}\sqrt{k_{b,AC}} = 0.26$.

There are two pathways in going from A → D ($His_{82}$-$Fe^{3+}$-$His_{18}$ → $Met_{80}$-$Fe^{2+}$-$His_{18}$), depending on whether the ligand exchange occurs prior to or after the electron transfer. These two pathways are shown in Scheme 1. For the A → B → D pathway, the $E^{0\prime}_{AD}$ can easily be derived with the Nernst equation:

$$E^{0\prime}_{AD} = E^{0\prime}_{AB} + 0.059 \cdot \log K_{BD} \quad (14)$$

For the A → C → D pathway:

$$E^{0\prime}_{AD} = E^{0\prime}_{CD} + 0.059 \cdot \log K_{AC} \quad (15)$$

If, during the time scale of the cyclic voltammetric experiments, all the reactions were fast, reversible, and at equilibrium, a single reversible couple at $E^{0\prime}_{AD}$ would be observed. In Figure 4 the cyclic voltammetry of the Phe82His variant shows two apparent redox couples: the quasi-reversible C/D couple of $Met_{80}$-$Fe^{2+/3+}$-$His_{18}$ at $E^{0\prime} \simeq +229$ mV and the A/B couple of $His_{82}$-$Fe^{3+/2+}$-$His_{18}$ with $E^{0\prime} \simeq -149$ mV form. The 2 × 2 mechanism predicts that these observed and apparent redox couples result from the sluggish conversion of A ⇄ C (see the equilibrium shown in eq 7). As a result of the relatively fast scan rate, A ($His_{82}$-$Fe^{3+}$-$His_{18}$) is not converted to C rapidly enough, and at negative enough potentials, the direct reduction of A → B occurs. Once formed, B rapidly rearranges to D, and for this reason no peak current for B → A is seen on the reverse scan (see Figure 4, peak B → A). As discussed earlier, reducing the scan rate causes the relative peak current for the positive C → D couple to increase because of ligand-exchange equilibrium within the oxidized state. This trend is seen in Figure 5. As the scan rate is increased from 10 to 100 and to 500 mV/s, we "catch up" with the equilibrium process and observe a substantial decrease in C → D peak. The relative heights of the two positive peaks, C → D and A → B, change as expected when too little time is permitted for the A ⇄ C equilibrium to provide C.

The thermodynamic values for the A → C → D pathway ($E^{0\prime}_{CD}$, $K_{AC}$) can be estimated, if we assume that $E^{0\prime}_{CD} \approx E^{0\prime}$ of the $Met_{80}$/$His_{18}$ form is 247 mV. This latter $E^{0\prime}$ is the *thermodynamic equilibrium* reduction potential for a typical Phe82 mutant (Phe82Ser) (*48*) which is in the $Met_{80}$-$Fe^{3+/2+}$-$His_{18}$ form in both oxidation states. By using this value of $E^{0\prime}_{CD}$ and the simulated value for $E^{0\prime}_{AD}$ in eq 15, one obtains a value of $K_{AC} = 0.06$. It has not been possible so far to experimentally measure the equilibrium constant for $K_{AC}$, seen in Figure 4 as peak A → C and its associated A ⇄ C equilibrium. As mentioned earlier, the simulated value for $K_{AC}\sqrt{k_{b,AC}}$ was 0.26. By using $K_{AC}$ along with this best fit value of $K_{AC}\sqrt{k_{b,AC}}$, $k_{f,AC} \simeq 1.0$ s$^{-1}$ and $k_{b,AC} \simeq 17$ s$^{-1}$ were calculated. A complete fit using these parameters is shown as the solid line in Figure 4. Figure 5 compares side by side the observed voltammetry and the simulation at three different scan rates. These results are summarized in Table 3.

Table 3: Thermodynamic Results for the Phe82His Interconversions Shown in Scheme 1 as Determined by Simulation of the Cyclic Voltammetric Data

| coordination form/redox couple | thermodynamic equilibrium reduction potentials |
|---|---|
| $His_{82}$-$Fe^{3+/2+}$-$His_{18}$ | $E^{0\prime}_{CD} = 47$ mV[a] |
| $Met_{80}$-$Fe^{3+/2+}$-$His_{18}$ | $E^{0\prime}_{CD} = 247$ mV[a] |
| $His_{82}$-$Fe^{3+}$-$His_{18}$ + $e^- \rightarrow$ $Met_{80}$-$Fe^{2+}$-$His_{18}$ | $E^{0\prime}_{AD} = 176$ mV |

[a] Assumed and simulation consistent $E^{0\prime}$ values based on the $E^{0\prime}$ of a semisynthetic $His_{82}$-$Fe^{3+/2+}$-$His_{18}$ cyt *c* (*49*) and the $E^{0\prime}$ of a typical and stable Phe82 variant, Phe82Ser cyt *c* (*48*), respectively. Equilibrium constants and first-order rate constants: $K_{AC} = 0.062$, $k_{b,AC} = 17$ s$^{-1}$, $k_{f,AC} = 1.0$ s$^{-1}$.

Analysis of the second or negative couple was limited because of the absence of a reverse current peak. Since we know $E^{0\prime}_{AD}$ with some certainty, we can calculate the value for $K_{BD}$ and make a reasonable assumption regarding $E^{0\prime}_{AB}$ (see eq 14). The semisynthetic Met80His mutant (*49*) of horse cyt *c*, which is in the His/His form in both redox states, has an $E^{0\prime} = 47$ mV. It can be tentatively assumed that $E^{0\prime}_{AB} = E^{0\prime}_{His80/His18} \approx 47$ mV. This $E^{0\prime}$ serves as a good approximation for the thermodynamic equilibrium reduction potential for a stable His-Fe-His form. From eq 14 for $E^{0\prime}_{AD}$ and the well-chosen $E^{0\prime}_{AB}$, $K_{BD} \simeq 3.6 \times 10^5$ was calculated. The position and shift of the negative peak, therefore, are mostly controlled by the slow electron transfer for the $His_{82}$-$Fe^{3+/2+}$-$His_{18}$ redox couple. For $k_{f,BD}$, since no reverse current (peak B → A) is seen even at 500 mV/s and considering the half-life of the species $His_{82}$-$Fe^{2+}$-$His_{18}$ starting at the switching potential of −600 mV, $k_{f,BD} > 10$ s$^{-1}$ and is likely to be faster.

Nonetheless, because of the correlations between $E^{0\prime}_{AB}$, $K_{BD}$, the heterogeneous electron-transfer rate for the A/B couple, $k_{s,AB}$, and $k_{f,BD}$, it is not possible to determine unambiguously a unique and meaningful combination of these values to inform us about the negative A/B couple. The position of the wave (couple) is completely determined by the kinetics of the electron transfer, $k_{s,AB}$, and the rate of the B → D conversion via $k_{f,BD}$. If these rates were very fast, thus permitting equilibrium to be achieved at each potential during the scan, only one voltammetric wave would appear at the thermodynamic potential of $E^{0\prime}_{AD} = 176$ mV vs SHE, which is close to where the first, positive C/D wave appears. Thus, there is no true thermodynamic information on the second negative A/B wave. Nonetheless, for simulation purposes, the values of $K_{BD}$ and $k_{f,BD}$ were calculated from eq 14 and are given in the legends of Figures 4 and 5. However, one should not ascribe any significant importance to these values. These latter results are consistent with the simulation, but there are other solutions that would also be

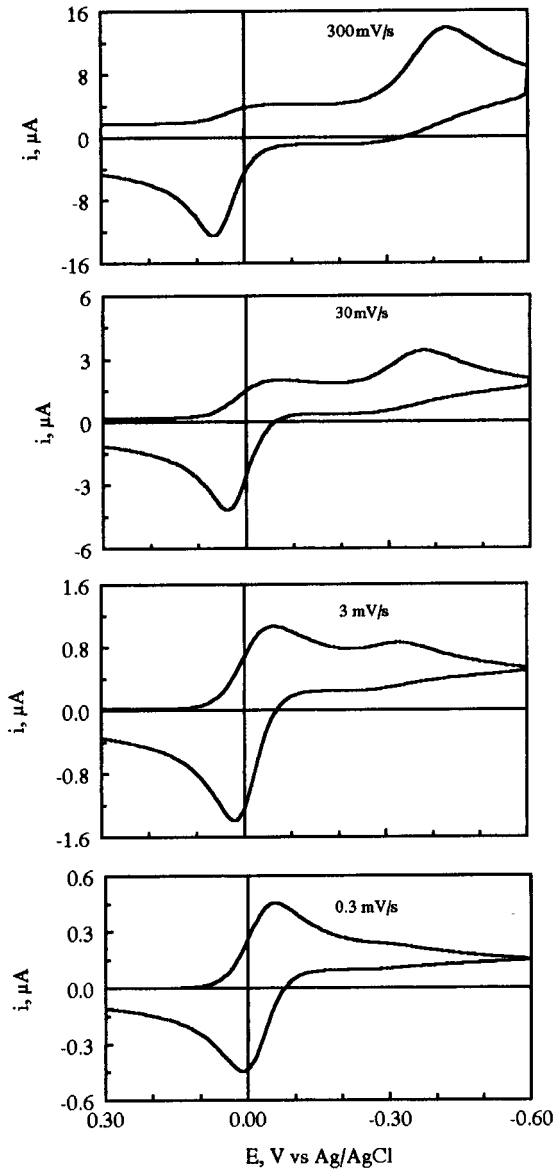


FIGURE 6: Digital simulations of the hypothetical cyclic voltammetry experiments from moderate to very slow scan rates: 300, 30, 3, and 0.3 mV/s. Potentials are versus Ag/AgCl.

consistent. It is the nearly reversible redox couple for which we have the most quantitative information. What these results do demonstrate is the complexity of the 2 × 2 mechanism and the need to be cautious regarding what can and cannot be determined with certainty. Experimental determination of $K_{AC}$ and faster scan rates to observe B → A will eliminate most of these uncertainties.

*Collapse of "Apparent Redox Couples" to One Net "Mixed" Redox Couple in the 2 × 2 Mechanism.* Two "apparent" and shifted redox couples, $His_{82}$-$Fe^{3+/2+}$-$His_{18}$ and $Met_{80}$-$Fe^{3+/2+}$-$His_{18}$, are observed by virtue of the nonequilibrium nature of the cyclic voltammetric scan; i.e., the various species are not in equilibrium (see Figures 4 and 5). To demonstrate that there is only one net "mixed" redox couple, simulations of the 2 × 2 mechanism were done using the results shown in Table 3, including the "well-chosen" thermodynamic equilibrium reduction potentials for the $His_{82}$-$Fe^{3+/2+}$-$His_{18}$ and $Met_{80}$-$Fe^{3+/2+}$-$His_{18}$ couples. Only the scan rate was varied from 300 mV/s to a very slow 0.3 mV/s (see Figure 6). At the extremely slow scan rate of 0.3 mV/s where equilibrium conditions are nearly achieved at each point during the scan, the two apparent redox couples were observed to collapse to one net redox couple: $His_{82}$-$Fe^{3+}$-$His_{18}$ + e ⇄ $Met_{80}$-$Fe^{2+}$-$His_{18}$ with $E^{0\prime}_{AD}$ = 176 mV. The results of these de novo simulations further confirm the 2 × 2 mechanism presented here.

*Unlikely Participation of an Alkaline Form of the Phe82His/Cys102Ser Mutant*

*Influence of Phe82 Mutations.* Earlier work (*5*, *42*, *43*) has shown that substitution of Phe82 with either Ser, Gly, Leu, or Ile residues lowers the p$K_a$ for the alkaline isomerization of iso-1-cyt *c* from a value of 8.5 for the wild-type protein to as low as 7.2 for Phe82Ile. The authors concluded that one critical role for the native Phe82 is the stabilization of the native heme binding environment. In this isomerization Met80 is substituted by a new ligand, most likely lysine 79 (*6*). For the Phe82His variant, in contrast to all of the above mutants, the p$K_a$ of the alkaline isomerization cannot be evaluated. The reason for this is that the form in the oxidized state is $His_{82}$-$Fe^{3+}$-$His_{18}$, and it does not possess the requisite 695-nm spectroscopic band of the $Met_{80}$-Fe bond which is used to follow the alkaline transition p$K_a$. Since the Phe82His variant is already in the $His_{82}$-$Fe^{3+}$-$His_{18}$ form, it can be viewed as an engineered oxidized "alkaline form". Additionally, in the earlier EPR study of the Phe82His variant (*19*), there was no evidence of Lys-$Fe^{3+}$-$His_{18}$ coordination. The similarity of the simulated and experimental cyclic voltammograms in Figure 5 also does not indicate the participation of an additional coordinating form. It is likely, but not unequivocal, that the $His_{82}$-$Fe^{3+}$-$His_{18}$ form precludes other isomerizations from occurring at pH 7, except the observed equilibrium/ligand exchange: $Met_{82}$-$Fe^{3+}$-$His_{18}$ ⇄ $His_{82}$-$Fe^{3+}$-$His_{18}$ (eq 7).

*Entropic Contributions to $E^{0\prime}$ and Intramolecular Rearrangement.* The $\Delta S^{0\prime}_{Rxn}$ determinations for wild-type horse cyt *c* (see Table 1) demonstrated the accuracy and precision of the SW voltammetric determination of $\Delta S^{0\prime}_{Rxn}$ and the suitability of this method for $\Delta S^{0\prime}_{Rxn}$ determination for iso-1-cyt *c* and its Phe82His variant. The quasi-reversible redox couple (C/D) of the Phe82His variant of iso-1-cyt *c* and the reversible couple of the wild-type were examined at various temperatures to determine their $\Delta S^{0\prime}_{Rxn}$. These results are summarized in Table 2. The experimentally determined entropy of reaction of the variant corresponds to that for the net (cross) redox reaction: $His_{82}$-$Fe^{3+}$-$His_{18}$ + $e^-$ → $Met_{80}$-$Fe^{2+}$-$His_{18}$ with $E^{0\prime} = E^{0\prime}_{AD}$.

For wild-type iso-1-cyt *c* and its Phe82His variant, the experimental values for $\Delta S^{0\prime}_{Rxn}$ were determined as −52 and −80 J/mol·K, respectively. Furthermore, each $\Delta S^{0\prime}_{Rxn}$ can be written as the appropriate difference in standard entropies of the reduced and oxidized form of the protein:

$$\Delta S^{0\prime}_{Rxn:VAR} = -80 \text{ J/mol·K} = S^{0\prime}_{Red,Met/His/VAR} - S^{0\prime}_{Ox,His/His/VAR}$$

$$\Delta S^{0\prime}_{Rxn:WT} = -52 \text{ J/mol·K} = S^{0\prime}_{Red,Met/His/WT} - S^{0\prime}_{Ox,Met/His/WT}$$

One can visualize how the individual standard entropies are relevant in the interpretation of the redox driven

molecular rearrangement. It is known that *reduced* wild-type cyt *c* compared to the oxidized form has the greater stability, e.g. it requires a higher concentration of guanidine hydrochloride to unfold, is more compact, and has greater resistance to proteolytic digestion (*50*). While it is likely that this is also true for the reduced mutant, its stability has not yet been determined. The negative entropy of reaction of cyt *c* and iso-1-cyt *c* has been attributed to greater solvation of the reduced protein compared to the oxidized form (*36, 51*), which, in turn, appears to be associated with its greater stability. Stronger $Met_{80}$-$Fe^{2+}$ coordination has also been proposed (*16, 17*). It is reasonable to assume that the $S^{0\prime}_{Red,Met/His:WT}$ and $S^{0\prime}_{Red,Met/His:VAR}$ are very similar. At the worst, using earlier observations that other noninterconverting Phe82 mutants (*42, 43*) have lower alkaline p$K_a$ values, it is expected that the reduced variant is actually more disordered and more open than wild-type protein: $S^{0\prime}_{Red,Met/His:VAR} \geq S^{0\prime}_{Red,Met/His:WT}$. Further support for the latter case is the observation that the reduced Phe82His variant is oxidized by air about 10 times faster than the wild-type cytochrome (*20*), suggesting that the reduced variant in the Met/His form is more open and disordered compared to the wild-type. If $S^{0\prime}_{Red,Met/His:VAR} \geq S^{0\prime}_{Red,Met/His:WT}$, then $S^{0\prime}_{Ox,His/His,VAR}$ is necessarily more than 30 J/mol·K more positive than the value for the wild-type protein ($S^{0\prime}_{Ox,Met/His,WT}$). Thus, the $His_{82}$-$Fe^{3+}$-$His_{18}$ form is 30 J/mol·K more disordered than the wild-type. This interpretation of the entropic contributions to the reduction reactions provides some qualitative insight into why the reaction His-$Fe^{2+}$-His → Met-$Fe^{2+}$-His is quite fast. While not formally linking differences in standard entropies to kinetics, we predict that $k_{f,BD}$ is much faster than 10 $s^{-1}$.

The $Met_{80}$-$Fe^{2+}$-$His_{18}$ form of the wild-type cyt *c* is certainly the most stable or lowest-conformational energy form of the protein (*50*). The standard entropy of the oxidized variant, $S^{0\prime}_{Ox,His/His:VAR}$, is quite positive, thus indicating that the $His_{82}$-$Fe^{3+}$-$His_{18}$ is by far the most disordered form. Upon reduction to the His-$Fe^{2+}$-His form, this new transient form is momentarily still "open and disordered" from its previous oxidized state. The His-$Fe^{2+}$-His form, in some ways, can be viewed as an "entatic" state that can easily collapse to the more stable Met-$Fe^{2+}$-His form: $His_{82}$-$Fe^{3+}$-$His_{18}$ (disordered but stable) + $e^-$ → $His_{82}$-$Fe^{2+}$-$His_{18}$ (disordered, transient) → $Met_{80}$-$Fe^{2+}$-$His_{18}$ (ordered, stable). In contrast, for $Met_{80}$-$Fe^{3+}$-$His_{18}$ → $His_{82}$-$Fe^{3+}$-$His_{18}$ coordination change, the reverse is true. The cyt *c* must first obtain a new and more disordered conformation, no doubt facilitated by the Phe82His variation itself. The product, $His_{82}$-$Fe^{3+}$-$His_{18}$, is then stabilized in the last steps of the reaction by His82 coordination to $Fe^{3+}$ heme, unlike all other Phe82 variants.

In regard to the forces which drive these rearrangements, it is well-known that the methionyl 80 sulfur prefers coordination to the $Fe^{2+}$ heme and histidine prefers the $Fe^{3+}$ heme in cytochromes *c* (*16*−*18*). These specific oxidation state dependent-coordination preferences appear to stabilize each final product and also drive the rearrangement upon change in redox state. Work presented here on the redox driven changes in axial coordination of the Phe82His mutant imitate quite well the redox driven changes noted in the Introduction for cytochrome $cd_1$ nitrite reductase. Upon reduction of $His_{82}$-$Fe^{3+}$-$His_{18}$ form to $His_{82}$-$Fe^{2+}$-$His_{18}$ form, the neighboring Met80 thermodynamically prefers coordination to the $Fe^{2+}$ heme, and this apparently initiates protein rearrangement and changes in axial coordination. These changes also demonstrate the remarkable flexibility of the protein chain in the region of Met80 through Phe(His)82. In light of this flexibility, new cyt *c* "molecular switches" are now being prepared and evaluated.

## ACKNOWLEDGMENT

We thank Robert Ponton for the fabrication of the temperature-controlled reference and working cell assemblies.

## REFERENCES

1. Wuttke, D. S., and Gray, H. B. (1993) *Cur. Opin. Struct. Biol. 3*, 555−563.
2. Moore, G. R., and Pettigrew, G. W. (1990) *Cytochromes c: Evolutionary, Structural and Physicochemical Aspects*, Springer-Verlag, Berlin.
3. Wallace, C. J. A., and Clark-Lewis, I. (1992) *J. Biol. Chem. 267*, 3852−3861.
4. Raphael, A. L., and Gray, H. B. (1989) *Proteins 6*, 338−340.
5. Barker, P. D., and Mauk, G. (1992) *J. Am. Chem. Soc. 114*, 3619−3624.
6. Ferrer, J. C., Guillemette, J. G., Bogumil, R., Inglis, S. C., Smith, M., and Mauk, A. G. (1993) *J. Am. Chem. Soc. 115*, 7505−7508.
7. Mines, G. A., Pascher, T., Lee, S. C., Winkler, J. R., and Gray, H. B. (1996) *Chem. Biol. 3*, 491−497.
8. Pascher, T., Chesick, J. P., Winkler, J. R., and Gray, H. B. (1996) *Science 271*, 1558−1560.
9. Williams, P. A., Fulop, V., Garman, E. F., Saunders, N. F. W., Ferguson, S. J., and Hajdu, J. (1997) *Nature 389*, 406−412.
10. Elove, G. A., Bhuyan, A. K., and Roder, H. (1994) *Biochemistry 33*, 6925−6935.
11. Colon, W., Elove, G. A., Wakem, L. P., Sherman, F., and Roder, H. (1996) *Biochemistry 35*, 5538−5549.
12. Takahashi, S., Yeh, S.-R., Das, T. K., Chan, C.-K., Gottfried, D. S., and Rousseau, D. L. (1997) *Nat. Struct. Biol. 4*, 44−50.
13. Yeh, S.-R., Takahashi, S., Fan, B., and Rousseau, D. L. (1997) *Nature Struct. Biol. 4*, 51−56.
14. Cutler, R. L., Pielak, G. J., Mauk, A. G., and Smith, M. (1987) *Protein Engin. 1*, 95−99.
15. Gao, Y., Boyd, J., Williams, R. J. P., and Pielak, G. J. (1990) *Biochemistry 29*, 6994−7003.
16. Margoliash, E., and Schejter, A. (1966) *Adv. Protein Chem. 21*, 126−213.
17. George, P., and Schejter, A. (1964) *J. Biol. Chem. 239*, 1504−1508.
18. Schejter, A., and Aviram, I. (1969) *Biochemistry 8*, 149−153.
19. Hawkins, B. K., Hilgen-Willis, S., Pielak, G. J., and Dawson, J. H. (1994) *J. Am. Chem. Soc. 116*, 3111−3112.
20. Schejter, A., Taler, G., Navon, G., Liu, X.-J., and Margoliash, E. (1996) *J. Am. Chem. Soc. 118*, 477−478.
21. Pielak, G. J., Boyd, J., Moore, G. R., and Williams, R. J. P. (1988) *Eur. J. Biochem. 177*, 167−177.
22. Ramely, L., and Krause, M. S., Jr. (1969) *Anal. Chem. 41*, 1362−1365.
23. Osteryoung, J., and O'Dea, J. J. (1986) in *Electroanalytical Chemistry: A Series of Advances* (Bard, A. J., Ed.) Vol. 14, pp 209−308, Marcel Dekker, Inc., New York.
24. Osteryoung, J. G., and Osteryoung, R. A. (1985) *Anal. Chem. 57*, 101−110.
25. Smith, E. T., and Feinberg, B. A. (1990) *J. Biol. Chem. 265*, 14371−14376.
26. Smith, E. T., Bennett, D. W., and Feinberg, B. A. (1991) *Anal. Chim. Acta 251*, 27−33.
27. Feinberg, B. A., Lo, X., Iwamoto, T., and Tomich, J. M. (1997) *Protein Sci. 10*, 69−75.

28. Tong, J., and Feinberg, B. A. (1994) *J. Biol. Chem. 269*, 24920−24927.
29. Rudolph, M. (1995) in *Physical Electrochemistry: Principles, Methods, and Applications* (Rubinstein, I., Ed.) pp 81−129, Marcel Dekker, Inc., New York.
30. Rudolph, M. (1990) *J. Electroanal. Chem. 292*, 1−7.
31. Rudolph, M., Reddy, D. P., and Feldberg, S. W. (1994) *Anal. Chem. 66*, A589−A600.
32. Taniguchi, I., Toyosawa, K., Yamaguchi, H., and Yasukouchi, K. (1982) *J. Chem. Soc., Chem. Commun.* 1032−1033.
33. Burrows, A. L., Guo, L.-H., Hill, H. A. O., McLendon, G., and Sherman, F. (1991) *Eur. J. Biochem. 202*, 543−549.
34. Yee, E. L., Cave, R. J., Guyer, K. L., Tyma, P. D., and Weaver, M. J. (1979) *J. Am. Chem. Soc. 116*, 1131−1137.
35. Taniguchi, V., Sailasuta-Scott, N., Anson, F. C., and Gray, H. B. (1980) *Pure Appl. Chem. 52*, 2275−2281.
36. Bertrand, P., Mbarki, O., Asso, M., Blanchard, L., Guerlesquin, F., and Tegoni, M. (1995) *Biochemistry 34*, 11071−11079.
37. Maniatis, T., Fritsch, E. F., and Sambrook, J. (1989) *Molecular Cloning: A Laboratory Manual*, Cold Spring Harbor Laboratory, New York.
38. Koshy, T. I., Luntz, T. L., Garber, E. A. E., and Margoliash, E. (1992) *Protein Express. Purif. 3*, 441−452.
39. Broach, J., Strathern, J., and Hicks, J. (1979) *Gene 8*, 121−133.
40. Wang, Y., and Margoliash, E. (1995) *Biochemistry 34*, 1948−1958.
41. Schejter, A., Koshy, T. I., Luntz, T. L., Sanishvili, R., Vig, I., and Margoliash, E. (1994) *Biochem. J. 302*, 95−101.
42. Rafferty, S. P., Pearce, L. L., Barker, P. D., Guillemette, J. G., Kay, C. M., and Smith, M. (1990) *Biochemistry 29*, 9365−9369.
43. Pearce, L. L., Gartner, A. L., Smith, M., and Mauk, A. G. (1989) *Biochemistry 28*, 3152−3156.
44. Liu, G., Shao, W., Zhu, S., and Tang, W. (1995) *J. Inorg. Biochem. 60*, 123−131.
45. Marchon, J.-C., Mashiko, T., and Reed, C. A. (1982) in *Electron Transport and Oxygen Utilization* (Ho, C., Ed.) pp 67−72, Elsevier Biomedical, New York.
46. Evans, D. H. (1990) *Chem. Rev. 90*, 739−751.
47. Balducci, G., and Costa, G. (1993) *J. Electroanal. Chem. 348*, 355−365.
48. Komar-Panicucci, S., Bixler, J., Bakker, G., Sherman, F., and McLendon, G. (1992) *J. Am. Chem. Soc. 114*, 5443−5445.
49. Raphael, A. L., and Gray, H. B. (1991) *J. Am. Chem. Soc. 113*, 1038−1040.
50. Schejter, A. (1996) in *Cytochrome c: A Multidisciplinary Approach* (Scott, R. A., and Mauk, A. G., Eds.) pp 335−345, University Science Books, Sausalito, CA.
51. Cohen, D. S., and Pielak, G. J. (1995) *J. Am. Chem. Soc. 117*, 1675−1677.
52. Margalit, R., and Schejter, A. (1970) *FEBS Lett. 6*, 278−280.

BI981037N